Brake and pneumatic wheel performance assessment – a new test rig

C Cantoni* M Gobbi** G Mastinu** A Meschini*

*Brembo SpA, via Brembo 25 Curno, Italy

**Politecnico di Milano, Department of Mechanical Engineering, via G La Masa, 1, Milan, Italy

Corresponding Author:

prof dr-ing Giampiero MASTINU

Politecnico di Milano, Department of Mechanical Engineering

Via Privata Giuseppe La Masa 1

20156 MILAN, Italy

e-mail: mastinu@mecc.polimi.it

tel. +39 333 326 79 07

fax +39 02 2399 8202

skype: giampiero.mastinu

Abstract

A fully new test rig is presented for the assessment of the physical performance of the primary vehicle safety system, namely pneumatic wheel and brake. For the accurate design of vehicle brake system, the need is to study not only the brake, but the brake & wheel assembly. This implies the accurate measurement of forces and moments applied both at the brake and at the wheel. This is a relatively complex and never attempted task in the known literature. The new test rig can be used both in the automotive and in the aerospace sectors. The test rig is basically a dynamometer with an unreferenced architecture, given by a special

arrangement of load cells. The test rig allows to measure, among other variables, the dissipated power at the brake and the dissipated power at the assembly composed by wheel and brake. The accurate modelling of the new test rig is performed, according to Industry 4.0 paradigms. Measurement uncertainties of the new test rig are analysed and it can provide excellent accuracy.

The dynamometer has shown that the pneumatic wheel itself may dissipate up to 30% of the power dissipated by the brake. This unreferenced result is relevant in both the automotive and aerospace fields.

Introduction

In the railway, aerospace or automotive industry, many applications do exist referring to dynamometers for measuring the torque and the deceleration performance of brakes. Especially in the automotive sector, a number of companies provide ready-to-use test-rigs [1-3]. The aim of the paper is to propose a new test rig with some additional features with respect to the current ones. Precisely, the role of the wheel, which appears to be crucial for brake design and development, is considered. The wheel dissipates some power and helps the brake transforming mechanical energy into heat. This occurrence has never been highlighted in the known literature and is the core topic of the paper.

Brake dynamometers belong to the broad class of chassis dynamometers [4]. We focus here on the sub-class of brake dynamometers, which can be divided into *two families.* The first family is typically composed by a motor, by a rotor with proper inertia, and by a brake. In the second family, a pneumatic wheel, rotating with the brake to be tested, rolls on a drum (with properly calibrated inertia), which is launched at a certain initial speed by a motor.

In the sequel, reference will be made to the second family of dynamometers.

The very first known dynamometer featuring brake&wheel was built for railway applications in 1891 by Southern Pacific Railroad [5]. The focus was on brake shoes pressed on the wheel rim. In [25, 35] recent

railway brake dynamometers are described which focus on brake only, since disk brakes and not shoe brakes are considered. The drag of the wheel is not taken into account, this topic would deserve some attention.

After the mentioned railway pioneering application, brake&wheel dynamometers where later employed in the aerospace sector. The concern was to consider the effect of the wheel providing proper deceleration to the landing aircraft. Thus, a number of recommendations have been developed for brake certification purposes [6-9], in which the brake&wheel assembly is included. The required measurements are limited to monitor the deceleration of the wheel, as stated in [17]. In [49,50] a well-known application is presented to test aircraft brakes according to the mentioned recommendations. In [51] an advanced large high-speed dynamometer for testing aircraft tyres, rim and brakes is presented which includes electrical simulation of the inertia. The considered load cells configuration makes this test rig quite different compared to the one presented in this paper. In [18], again in the aerospace sector, an indoor dynamometer is used to study the tyre wear due to braking, however the special measurements that we address in this paper are not addressed.

In the automotive sector the testing of brake&wheel is usually performed on the road, not indoor. This is due to the fact that it is relatively easy making a car running on a test track. This is not the case for aircrafts, which explains why indoor brake&wheel dynamometers have been developed in the aerospace sector.

Referring to the automotive sector, the following contributions have been given.

In [10], a brake&wheel test rig is presented, the focus is mainly on tyre characteristic measurement, brake development is not dealt with. In [11] a relatively simple test rig is introduced with flywheel and magnetic powder clutch to simulate friction at the wheel-ground interface. The focus is on ABS performance. The same goal on ABS is the key topic presented in [12,31] where a brake&wheel dynamometer or an adapted suspension system are employed. In [13] a complete test bench is proposed to test the vehicle brake performance, the focus is mainly on whole vehicle behaviour. In [16] a dynamometer is employed for correlating indoor results with vehicle brake tests, the focus is more on brake squeal than on brake safety function. In [34] a special type of brake dynamometer is dealt with, namely the so-called "roller brake

dynamometer". An accurate measurement of forces is addressed but the system proposed in [34] is devoted to certification purposes only, with reference to service provided by garages. In [23,24,27] a comprehensive and very accurate comparison among five brake dynamometers has been performed in order to detect how and why friction varies so unpredictably. Unfortunately, the brake dynamometers are not well described in the paper, they seem including the suspension system without the wheel. So, the actual total power seems dissipated by the brake only and, apparently, not by the pneumatic tyre as well. A number of brake dynamometers are cited in [27,28] (Dynamometer, Chase, Link, FAST, Ranzi Cuna, Ranzi LCR, and the Friction test machine from ATE), none of them have the same characteristics the test rig presented in this paper features. In [30], a brake&wheel dynamometer is developed but it requires the actual vehicle to be included in a "Hardware In the Loop" system, so the precise detection of relevant forces and dissipated powers are lost.

In [26, 29], two different brake dynamometers are employed with different aims (detecting electric vehicle braking power, detecting brake drag), no similarities with the test rig proposed in this paper can be found.

In [32,33] a general overview for electric brake dynamometers is given, in which the wheel losses are compensated by an electric motor, no influence of the longitudinal slip seems mentioned. The accurate definition of energy dissipated by such electric motor is crucial for brake performance assessment. In the test rig we propose such an issue is overcome by including the tyre into the dynamometer.

In [36] the requirements for a brake dynamometer for commercial vehicles are given, the specific characteristics of the test rig proposed in this paper are not mentioned.

A comprehensive set of test benches, useful to test brake&wheel, can be found in excellent academic Institutions [14,15]. The test rig proposed in this paper is very much dedicated to develop brakes, taking into account pneumatic wheel performance which makes it original with respect to the known experimental facilities.

In [19-22] instrumented spindles were used to detect forces at the brake&wheel assembly. In the test rig proposed in this paper, only single axis load cells have been employed, because Authors' experience has shown that for multi-axis load cells the cross talk is too high to perform accurate measurements [20-22].

The paper is organized as follows. Firstly, the concept design of the new dynamometer is presented. Then the layout and technical features of the new dynamometer are presented. Typical measurements are presented to show the capabilities of the new dynamometer. Finally, the measurement accuracy is analysed In the sequel, the term wheel will refers to the pneumatic wheel which rotates with the brake to be tested. The term drum refers to the roller on which the wheel is made rotating.

1. **Concept design of the brake&wheel dynamometer.**

In this section, we focus on the concept design of the brake& wheel dynamometer. We briefly describe the basic theory that underpins the design of dynamometers for brake&wheel performance assessment, and, in particular, the special dynamometer that we present in this paper.

In Fig. 1 the scheme of the dynamometer is shown. A pneumatic wheel is pressed on a drum and rotates with it. The drum is connected to a system (transmission and flywheels) that reproduces the inertia of the vehicle whom the brake under test belongs to. As the brake is activated, the wheel applies a longitudinal force to the drum that is decelerated until the rest condition is reached.
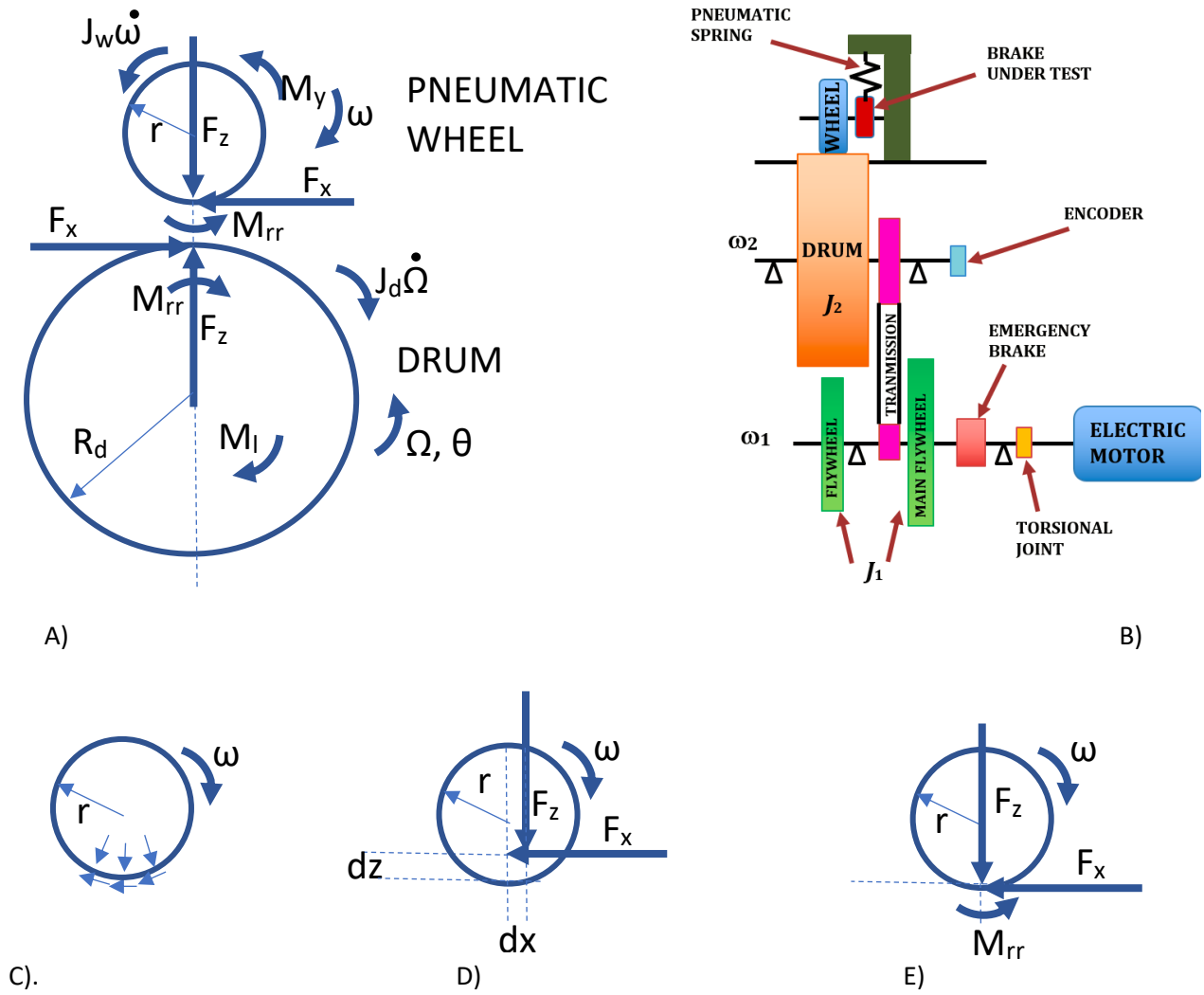
Fig.1. A) Scheme of brake&wheel dynamometer with forces at the wheel-drum interface. B) Scheme of brake&wheel dynamometer with transmission. C) Forces on the wheel, distributed at the contact patch between wheel and drum. D) Resultants of the forces shown in C). E) Forces and moments equivalent to the ones shown in D).

The equations of motion of the wheel and of the drum read

$$M_y + J_w \dot{\omega} - F_x r + M_{rr} = 0$$

$$F_x R_d + J_d \dot{\Omega} + M_l + M_{rr} = 0 \tag{1}$$

where the symbols, reported in Fig.1, have the following meaning

F_x longitudinal force

F_z radial force

M_y moment applied to the brake

M_l moment due to dissipation at the drum (e.g. aerodynamics, transmission, bearings)

M_{rr} moment due to rolling resistance

J_d moment of inertia of the drum (plus transmission and flywheels)

J_w moment of inertia of the wheel around its axis

ω angular speed of the wheel

Ω angular speed of the drum

The important quantities to be measured are:

- the deceleration of the drum, $d_d = d\, \Omega R_d /dt$ which corresponds to the linear deceleration of the vehicle to which reference is made

- the power dissipated by the brake&wheel system $P_d = F_x \, \Omega \, R_d + M_{rr} \, \Omega$

- the power dissipated by the brake only $P_w = M_y \, \omega = (-J_w \dot\omega + F_x r - M_{rr})\omega$

Now we provide a simple but important consideration that explains the key feature of the new dynamometer.

Let us concentrate on the dynamics of the wheel. Let us imagine that the kinematic variables, namely ω and $d\omega/dt$, and other parameters (J_w, , r) are known. By inspection of the first equation of system (1) (pertaining to the dynamic equilibrium of the wheel) we see that to gain an insight into the dynamic behaviour of the wheel, we should be able to monitor (i.e.to measure) at least *three* of the *four* terms of the equation (the fourth term can be derived from the other three by applying the equation - monitoring or measuring the whole four terms is costly and useless, and possibly adds uncertainty). In the present approach we measure F_x , M_{rr}, $J_w \dot\omega$ in a simple and effective way (see next Section). This gives an immediate understanding of the dynamic behaviour of the brake&wheel system. By measuring F_x, M_{rr} we have the core variables that allow

to immediately derive both the power dissipated by the brake&wheel system ($P_d = F_x \Omega R_d + M_{rr}\Omega$) and the power dissipated by the brake only ($P_w = (-J_w \dot{\omega} + F_x r - M_{rr})\omega$).

Usually, in current dynamometers F_x, and M_{rr} are not measured, instead M_y and F_z are measured. Usually, F_x is derived by the second equation of system 1, with missing information on M_l and M_{rr}. The measurement in current dynamometers is rather inaccurate and for this reason is not adopted in the application presented in this paper.

2. System layout and mathematical models of the dynamometer

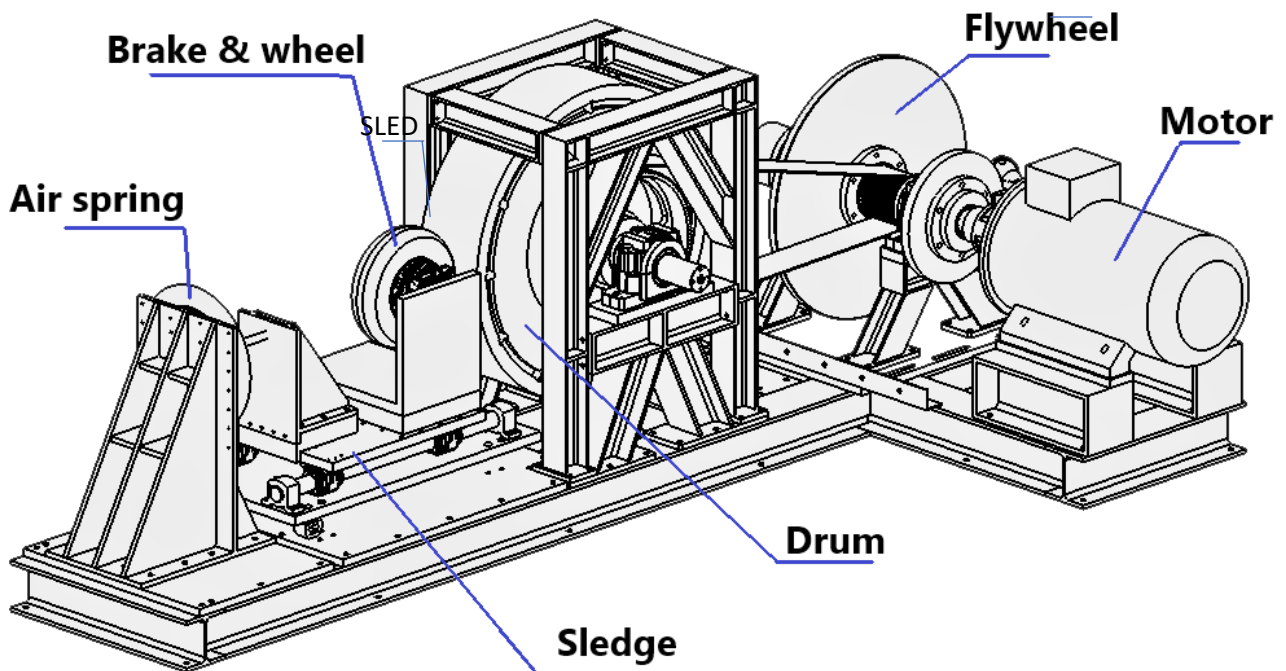The dynamometer is called BRAD (Brembo Aerospace / Automotive Dynamometer) and is shown in Fig.2.

Fig. 2. Overview of BRAD, a dynamometer for testing brake and wheel systems. Main assemblies: sledge, drum, transmission and flywheels, motor. The control box is not shown.

The system composed by brake plus wheel is positioned on a sled (Fig.3). When the brake is actuated, the wheel applies a longitudinal force on the drum which is decelerated down to stop.

Fig. 3. A brake&wheel system under test on BRAD.

The dynamometer can be divided into five main sub-systems: the sled, the drum, the transmission and the flywheels, the driving motor and the controller (Fig.1,2).

The sled is primarily responsible for the application of the radial load and the measurement of longitudinal force at the pneumatic wheel contact patch (wheel-drum interface). A pneumatic spring presses the wheel on the drum and provides a suspension system to filter the vibrations that arise due to the lack of roundness of the pneumatic wheel. The drum provides the running surface for the (pneumatic) wheel. Flywheels are used to simulate the inertia of the vehicle under consideration. Drum and flywheels define the amount of energy that will be dissipated by the brake during the deceleration. A motor is used to accelerate the drum to the required speed for the test. To limit the mass to be added to the drum, the flywheels are connected to the motor output shaft. A toothed belt reduces the angular speed of the motor to the requested angular

speed of the drum. The controller is used to manage and run the test, control the whole dynamometer (braking actuation included) and to acquire the signals coming from all the sensors of the dynamometer. The dynamometer was designed and constructed by Politecnico di Milano – Department of Mechanical Engineering.

The main characteristics of the dynamometer are summarized in Tab.1.

Table 1. Technical specification of the dynamometer.

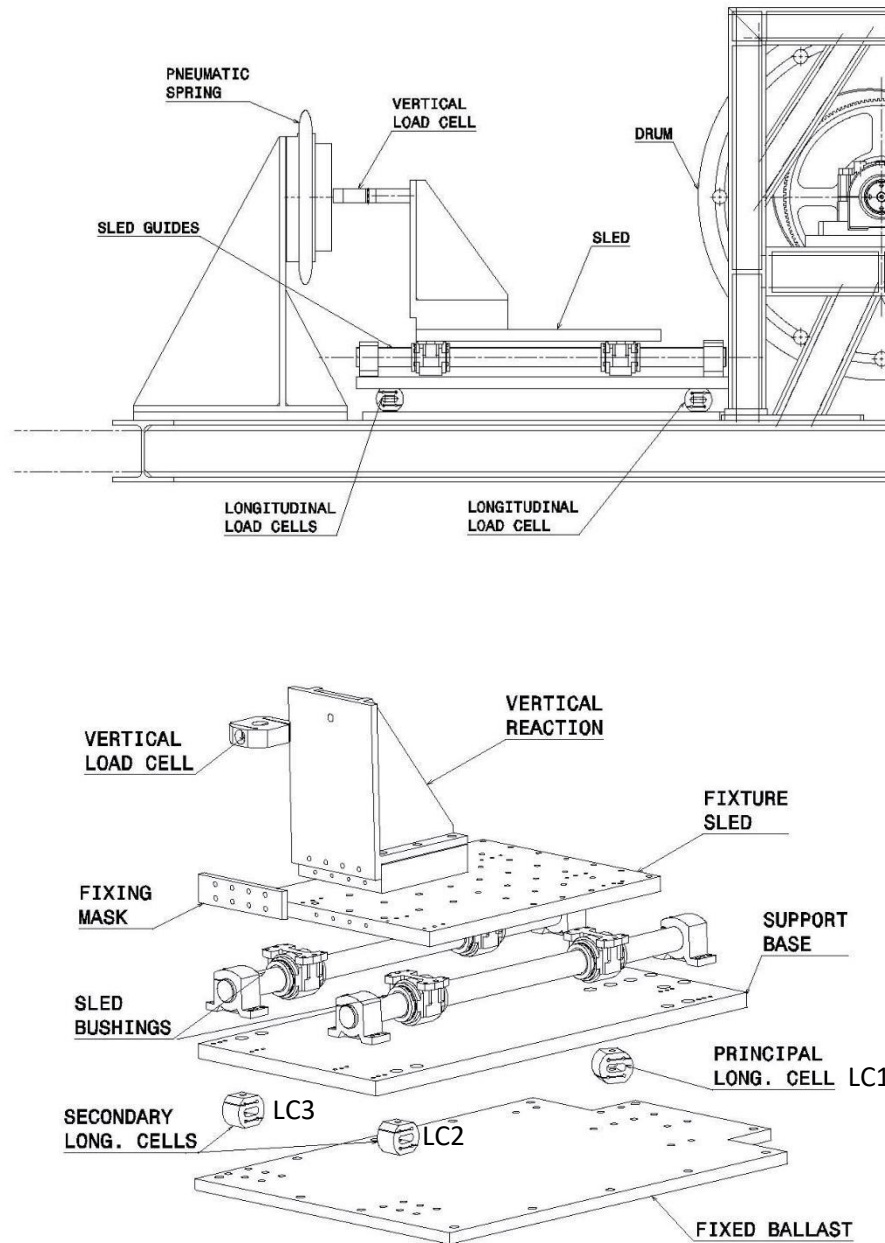| Parameter	Value	Note
Drum diameter	1.2 m	
Max. equivalent speed	250 km/h	
Reference equivalent mass	2220 kg	can be increased or decreased
Radial force	5-60 kN	on the wheel
Max. sled stroke	87 mm	
Max. tangential force	14 kN	at the drum surface
Max. deceleration	6.3 m/s^2 (0.64 g)	

2.1. Sled

Fig. 4. The sled of BRAD. The technical specifications of the sensors are reported in Appendix.

Fig.4. shows the sled. The sled (carrying the brake&wheel system) is displaced linearly towards the drum by

a pneumatic spring. The spring inflation pressure is controlled between 2 and 5 bar. The stiffness of the

spring is of the order of 100kN/m, quite weak if compared to the wheel radial stiffness. This allows to keep as constant as possible the radial force on the wheel.

The sled opposes no resistance to the force of the pneumatic spring due to linear guides ball bushings (sled bushings in Fig.4).

The sled is mounted on a statically determined system of constraints composed by four load cells (Fig.4). The load cell which applies the radial load on the wheel is called vertical (even if is measuring a horizontal force on the sled). The other three load cells are used to measure all the forces applied by the brake&wheel system to the drum.
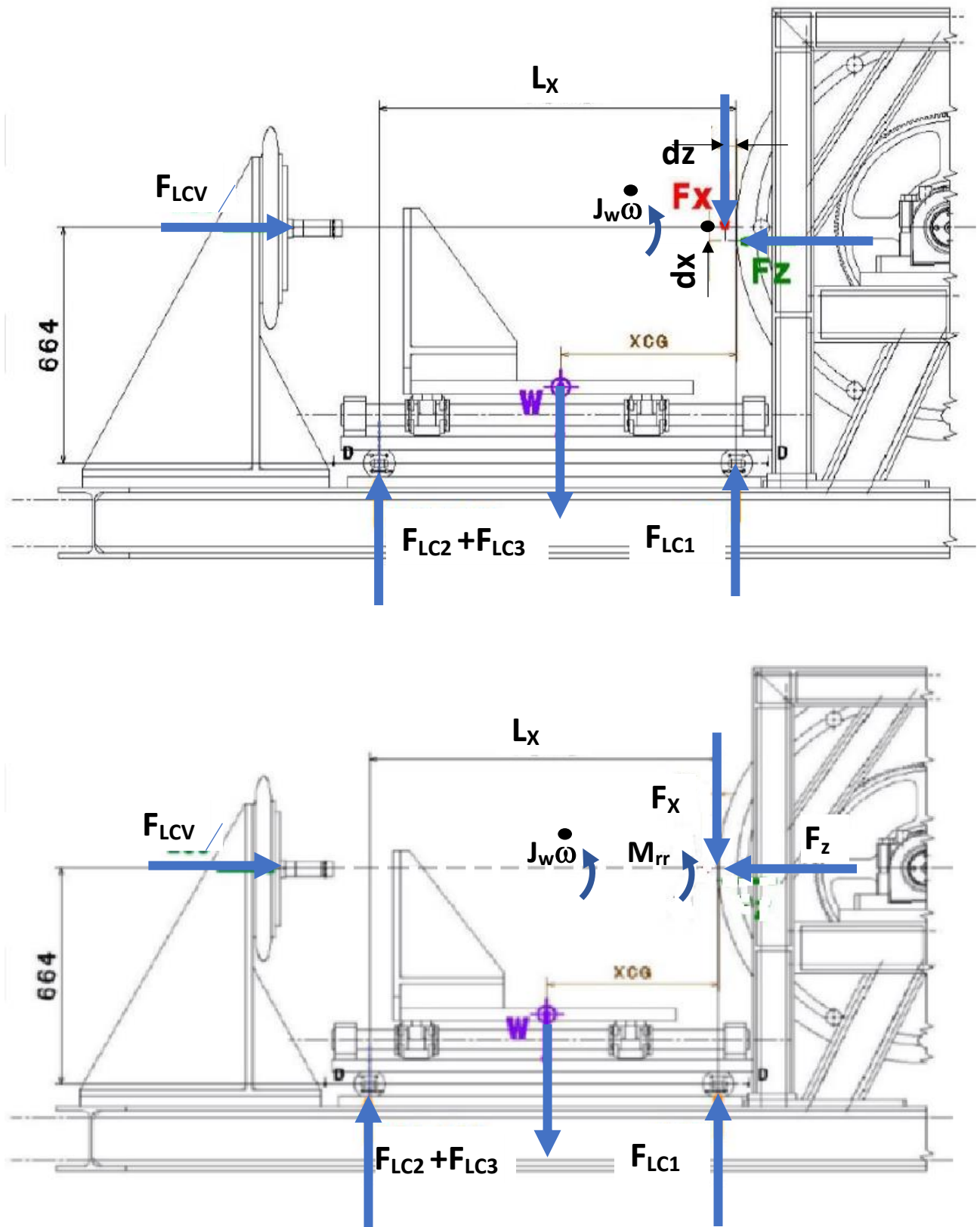
Fig. 5. The sled of BRAD with the external forces applied when a brake&wheel system (not shown) is under test. M_{rr} is shown in the bottom figure , for dx=dz=0.

The main load cell (detecting force F_{LC1}) is positioned in order to have its axis *tangential* to the drum surface.

This is a novel feature of the dynamometer, actually the load cell positioned in such a convenient place collects directly the force F_x which is the most important variable to be measured.

The equilibrium equations of the sled (plus brake&wheel system) can be written referring to forces in Fig 5

$$F_{LCV} = F_z$$

$$F_{LC1} + (F_{LC2} + F_{LC3}) = F_x + W$$

$$(F_{LC2}+F_{LC3})\,L_x + F_z*dx - F_x*dz - W*X_{CG} - J_w d\omega/dt = (F_{LC2}+F_{LC3})\,L_x - M_{rr} - W*X_{CG} - J_w d\omega/dt = 0$$

where F_{LCV} F_{LC1} F_{LC2} F_{LC3} are the forces given by load cells, W is the weight and L_x , X_{CG}, dx and dz are the geometrical distances depicted in Fig.5. Such dx and dz are not measured because their effects are considered in the moment M_{rr}. A generally accepted hypothesis is that $dz=0$.

X_{CG} can be derived when $Fx, = Fz = 0$ by mesurement as $X_{CG} = (F_{LC2\_static}+F_{LC3\_static})*L_x) / (F_{LC1\_static}+(F_{LC2\_static}+F_{LC3\_static})$

We have three unknowns, namely *Fx, Fz, M$_{rr}$*. Thus we have:

$$F_z = F_{LCV} \tag{2}$$

$$F_x = F_{LC1} + (F_{LC2}+F_{LC3}) - W \tag{3}$$

$$M_{rr} = - W*X_{CG} + (F_{LC2}+F_{LC3})\,L_x - J_w d\omega/dt \tag{4}$$

It is important to notice that the dynamometer allows to find the two variables that are relevant for the deceleration of a vehicle, namely F_x and M_{rr}. Actually, F_x is the only force that produces deceleration in a vehicle and M_{rr} is related to the so-called rolling resistance.

M_{rr} is easily measured by processing the forces F_{LC2} and F_{LC3}. The load cells LC2 and LC3 (which provide such F_{LC2} and F_{LC3} forces) are positioned in a convenient location to measure M_{rr}.

An in-depth analysis is presented in Section 4 dealing with how the new dynamometer allows to understand and measure not only the brake&wheel performance, but also how the brake itself actually works. Such an analysis is made possible by measuring accurately F_x and M_{rr}.

2.2 Drum

The drum is basically a solid cylinder with a running surface that can be simply steel or friction paper. The dimensioning of the drum has tight tolerances in order to avoid vibrations. The cylindrical error of the drum running surface is < 0.05 mm.

2.3 Transmission and flywheels

Most of the Inertia of the dynamometer is contained in the drum and in the flywheels (the biggest flywheel is called main flywheel, see Fig.1).

There are two different shafts (Fig.1): the high-speed shaft is the one driven by the motor where the main flywheel is mounted. The low speed shaft is the one that rotates together with the drum.

The two shafts are connected through a transmission belt with ratio equal to 3.056. The ratio is the results of the number of teeth on the small pulley (44) versus those on the bigger pulley (144).

The rotating masses of drum and flywheel simulate the mass of a given vehicle. Given the drum (d) and the flywheel (f) each rotating at their own rotational speed (ω), the kinetic energy can be written as:

$$E_k = E_k|_d + E_k|_f = \frac{1}{2} I_d\, \omega_d^2 + \frac{1}{2} I_f\, \omega_f^2$$

given $\omega_d = \dfrac{V}{R_d}$ and $\omega_f = \dfrac{\omega_d}{\tau_{df}}$

we can write $E_k = \dfrac{1}{2}\left(\dfrac{I_d}{R_d^2} + \dfrac{I_f}{\tau_{df}^2\,R_d^2}\right)V^2$

where

R_d = Drum radius

τ_{df} = Transmission Ratio

The equivalent mass of the vehicle is: $M_E = \dfrac{I_d}{R_d^2} + \dfrac{I_f}{\tau_{df}^2\,R_d^2}$

Table 2. Moment of inertia of single parts of the dynamometer and equivalent mass in a typical configuration.

Component	Mass	Mom. of Inertia	Transmission ratio	Equivalent mass
Emergency Brake Disc	58.0	1.9000	0.305556	56.5
Emergency Brake Flange	21.5	0.2700	0.305556	8.0
High Speed Shaft	62.0	0.0628	0.305556	1.9
1st Flywheel Flange	61.6	0.5820	0.305556	17.3
2nd Flywheel Flange	61.6	0.5820	0.305556	17.3
Small Pulley	20.6	0.1100	0.305556	3.3
Shafter 90 mm	4.5	0.0141	0.305556	0.4
Main Flywheel Disc	203.5	26.3100	0.305556	782.8
Drum	2544.3	476.0000	1.000000	1322.0
Big Pulley	108.4	5.8000	1.000000	16.1
Low Speed Shaft	80.0	0.1100	1.000000	0.3

2.4 Motor and inverter

A three-phase motor is attached to the high-speed shaft through a flexible joint. The motor has a built-in temperature monitoring system which activates additional cooling is necessary. A pneumatic emergency brake is connected to the shaft so that the dynamometer can be stopped in case any problem occurs during the test. The inverter is a 132kW SIEMENS - SINAMICS Power Module PM240-2.

Tab.3. Technical characteristics of the inverter of BRAD

	INPUT	OUTPUT
Number of phases	3	3AC
Nominal Line Voltage	380 V	400V
Nominal line frequency	50Hz	
Rated current (LO)	242 A	250 A
Rated current (HO)	218 A	205 A
Rated output Power (LO)		122 kW
Rated input Power (HO)		110 kW
Max output current		410 A
Pulse frequency		2kHz
Output frequency for vector control		0..200Hz

2.5 Controller

The control and acquisition system is based on a National Instruments cRIO 9035 and is able to handle analogue and digital signal both as input and output. The control is feedforward with threshold limit values for safety reasons.

In the operation mode, typically, the controller launches the drum which, in a few hundred seconds, reaches the steady state speed. Then the pneumatic spring is inflated and the wheel is pressed on the drum and accelerated. After few seconds, the brake is actuated and all the relevant variables are recorded. Threshold values refer to the stroke of the sled carrying the wheel, to the pressure inside the pneumatic spring, to the temperature of the brake, to the speed of the drum, and so on. Should threshold values not be respected (interlock), the control system slows down (with an emergency brake) the drum, and deflate the pneumatic spring to avoid contact of the wheel on the drum.

2.6 Vibrations

To assess the torsional eigenfrequencies of the system, a multi-body model has been developed. Fig.6 shows the model, the parameters of the model are listed in Tab. 4. To check the computations referring to the multi-body model, an AMESIM model has been used which is shown in Fig. 6. We did derive a proprietary software to describe the BRAD vibrations because we wanted to monitor the evolution of the dynamic behaviour of the test rig during its life. Actually a tuned proprietary model allows an easy monitoring of the aging by checking the variation of the identified parameters of the system.

Table 4. Parameters of the multi-body model.

Parameter	Description	Value
θ_1	Motor shaft rotation	-
θ_2	Brake disk rotation	-
θ_3	Driving pulley rotation	-
θ_4	Driven pulley rotation	-
θ_5	Flywheel rotation	-

|			
θ_6	Drum rotation	-	
J_m	Motor inertia	1.28	kg/m^2
J_B	Brake disk inertia	2.24	kg/m^2
J_{P1}	Driving pulley inertia	0.1	kg/m^2
J_{P2}	Driven pulley inertia	15	kg/m^2
J_f	Flywheel inertia	28.2	kg/m^2
J_{drum}	Drum Driving pulley inertia	470	kg/m^2
K_{ed}	Stiffness between the motor and the brake disk	5.56 E+04	Nm/rad
K_2	Stiffness between the brake disk and the driving pulley	9.15 E+06	Nm/rad
K_3	Stiffness between the driving pulley and the flywheel	4.40 E+06	Nm/rad
K_{belt}	Stiffness of the transmission belt	1.01 E+06	N/m
K_4	Stiffness between the driven pulley and the drum	2.64 E+06	Nm/rad
C_{eq}	Damping between the motor and the brake disk	122.7	Nms/rad
C_2	Damping between the brake disk and the driving pulley	6.4	Nms/rad
C_3	Damping between the driving pulley and the flywheel	6.4	Nms/rad
C_{belt}	Damping of the transmission belt	1.3	Ns/m
C_4	Damping between the driven pulley and the drum	17.1	Nms/rad
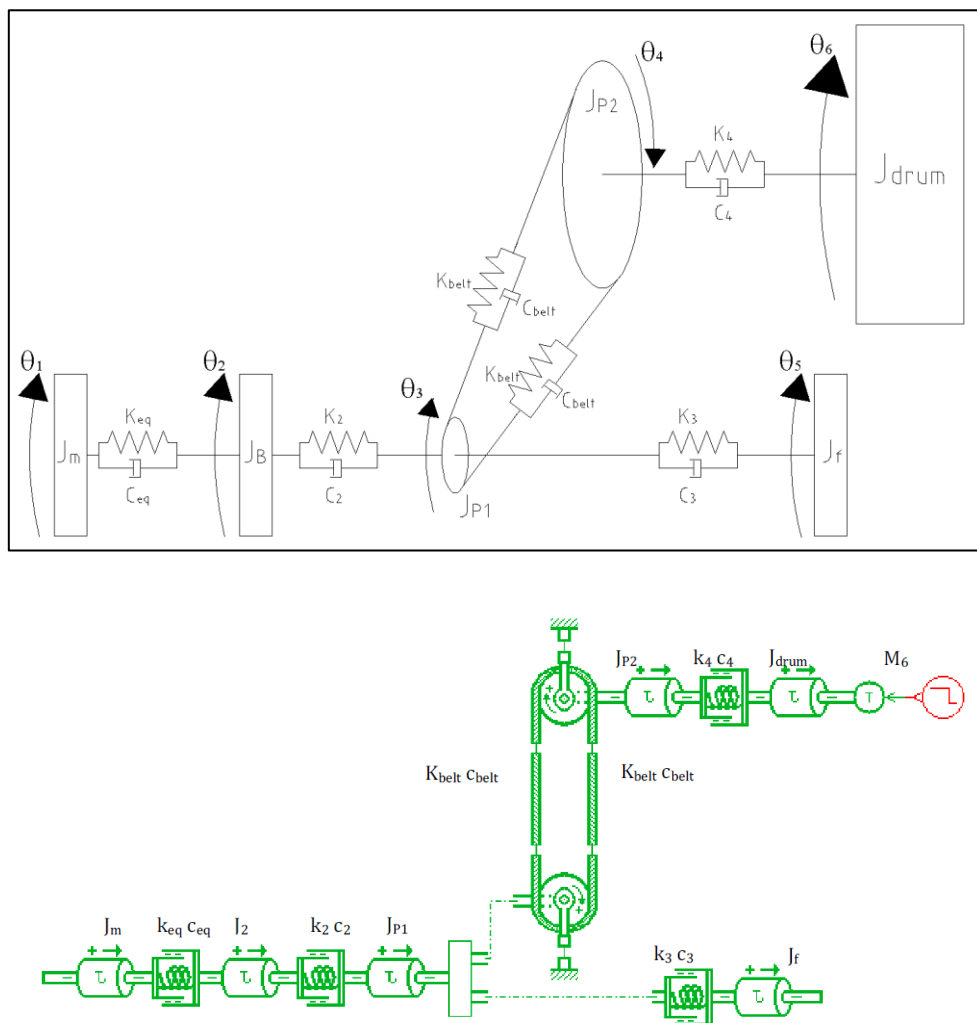
Fig. 6. Multi-body model for the analytical derivation of the equations of motion (top) and the corresponding AMESIM 1D model (bottom).

To calculate the system natural frequencies the following Lagrange equation can be used:

$$\frac{d}{dt}\left(\frac{\partial T}{\partial \dot{x}_i}\right) - \frac{\partial T}{\partial x_i} + \frac{\partial D}{\partial \dot{x}_i} + \frac{\partial V}{\partial x_i} = 0$$

where T, D and V are respectively the kinetic, damping and potential energy and x_i represent the d.o.f. of the system.

$$x = [\theta_1 \ \theta_2 \ \theta_3 \ \theta_4 \ \theta_5 \ \theta_6]^T$$

The kinetic energy T of the system reads

$$T = \frac{1}{2}J_m \dot{\theta}_1^2 + \frac{1}{2}J_B \dot{\theta}_2^2 + \frac{1}{2}J_{P1} \dot{\theta}_3^2 + \frac{1}{2}J_{P2} \dot{\theta}_4^2 + \frac{1}{2}J_f \dot{\theta}_5^2 + \frac{1}{2}J_{drum} \dot{\theta}_6^2$$

The potential energy V is

$$V = \frac{1}{2}K_{eq} \Delta\varphi_1^2 + \frac{1}{2}K_2 \Delta\varphi_2^2 + \frac{1}{2}K_3 \Delta\varphi_3^2 + \frac{1}{2}K_{belt1} \Delta L_{belt1}^2 + \frac{1}{2}K_{belt2} \Delta L_{belt2}^2 + \frac{1}{2}K_4 \Delta\varphi_4^2$$

where

$$\Delta\varphi_1 = \theta_1 - \theta_2$$

$$\Delta\varphi_2 = \theta_2 - \theta_3$$

$$\Delta\varphi_3 = \theta_3 - \theta_5$$

$$\Delta L_{belt1} = \Delta L_0 + R_{P2} \theta_4 - R_{P1} \theta_3$$

$$\Delta L_{belt2} = \Delta L_0 - R_{P2} \theta_4 + R_{P1} \theta_3$$

$$\Delta\varphi_4 = \theta_4 - \theta_6$$

The damping energy D can be written as:

$$D = \frac{1}{2} C_{eq} \, \Delta\dot{\varphi}_1^2 + \frac{1}{2} C_2 \, \Delta\dot{\varphi}_2^2 + \frac{1}{2} C_3 \, \Delta\dot{\varphi}_3^2 + \frac{1}{2} C_{belt1} \, \dot{\Delta L}_{belt1}^2 + \frac{1}{2} C_{belt2} \, \dot{\Delta L}_{belt2}^2 + \frac{1}{2} C_4 \, \Delta\dot{\varphi}_4^2$$

where

$$\Delta\dot{\varphi}_1 = \dot{\theta}_1 - \dot{\theta}_2$$

$$\Delta\dot{\varphi}_2 = \dot{\theta}_2 - \dot{\theta}_3$$

$$\Delta\dot{\varphi}_3 = \dot{\theta}_3 - \dot{\theta}_5$$

$$\dot{\Delta L}_{belt1} = R_{P2} \, \dot{\theta}_4 - R_{P1} \, \dot{\theta}_3$$

$$\dot{\Delta L}_{belt2} = R_{P2} \, \dot{\theta}_4 + R_{P1} \, \dot{\theta}_3$$

$$\Delta\dot{\varphi}_4 = \dot{\theta}_4 - \dot{\theta}_6$$

From the Lagrange equation, we obtain the motion equation of the system which has the form:

$$[J] \, \ddot{x} + [R] \, \dot{x} + [K] \, x = 0$$

The system natural frequencies values (measured in rad/s) correspond to the eigenvalues of the following

matrix A

$$A = \begin{bmatrix} - [M]^{-1} [R] & - [M]^{-1} [K] \\ [I] & [0] \end{bmatrix}$$

The calculated values of the torsional natural frequencies of the system are: 4 Hz, 33 Hz, 70 Hz, 100 Hz and

1164 Hz. Apart vanishing discrepancies, the same frequencies were found with the AMESIM model.

We derived the Frequency Response Functions (FRF) for both the multi-body model and the corresponding

AMESIM model. Again the correspondence between the two models was satisfactory. Fig. 7 shows the FRF

of the drum rotation when a unitary torque excitation is applied at the drum. Resonances must be

traversed quickly, the knowledge of such operating constraints allows proper operarion of the test rig.
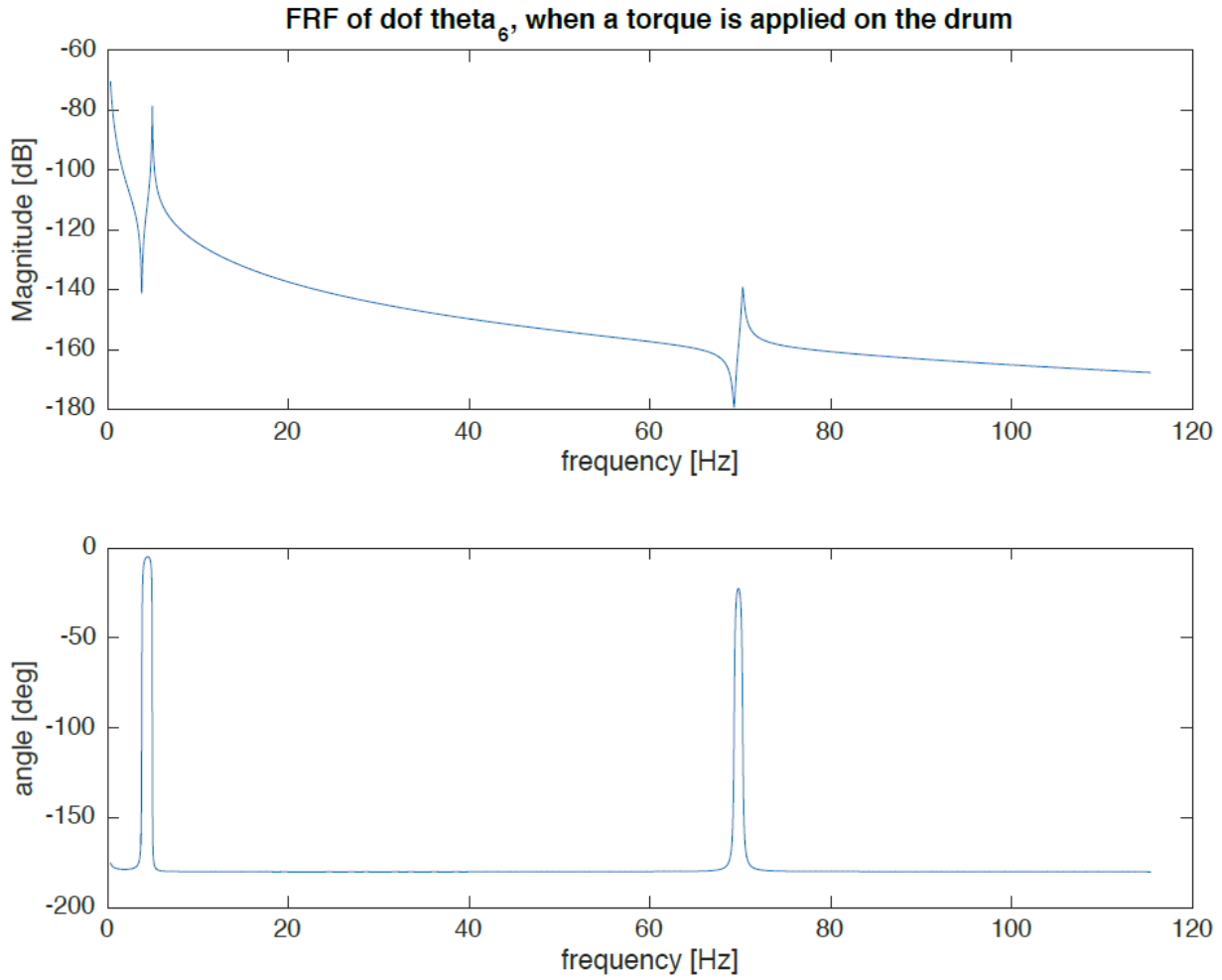
Fig. 7. Frequency response function (magnitude and phase angle) of the drum rotation (Θ_6 in Fig.6) when a unitary torque excitation is applied at the drum. System's data in Tab.4.

To find the structural natural frequencies of the dyno, a FEM model has been developed in the ABAQUS environment. All the physical parts of the structure have been modelled by means of beams and shell elements with the correct cross section and thickness (see Fig.8). The first relevant natural frequency of the dyno is about 32 Hz and it is related to the vibration of the fast shaft supports (see Fig. 8 C). This frequency corresponds to a drum peripherical speed of 133 km/h; during the preliminary test of the bench a vibration has been experienced around 130 km/h, the problem has been solved by a fine balancing of the fast shaft.
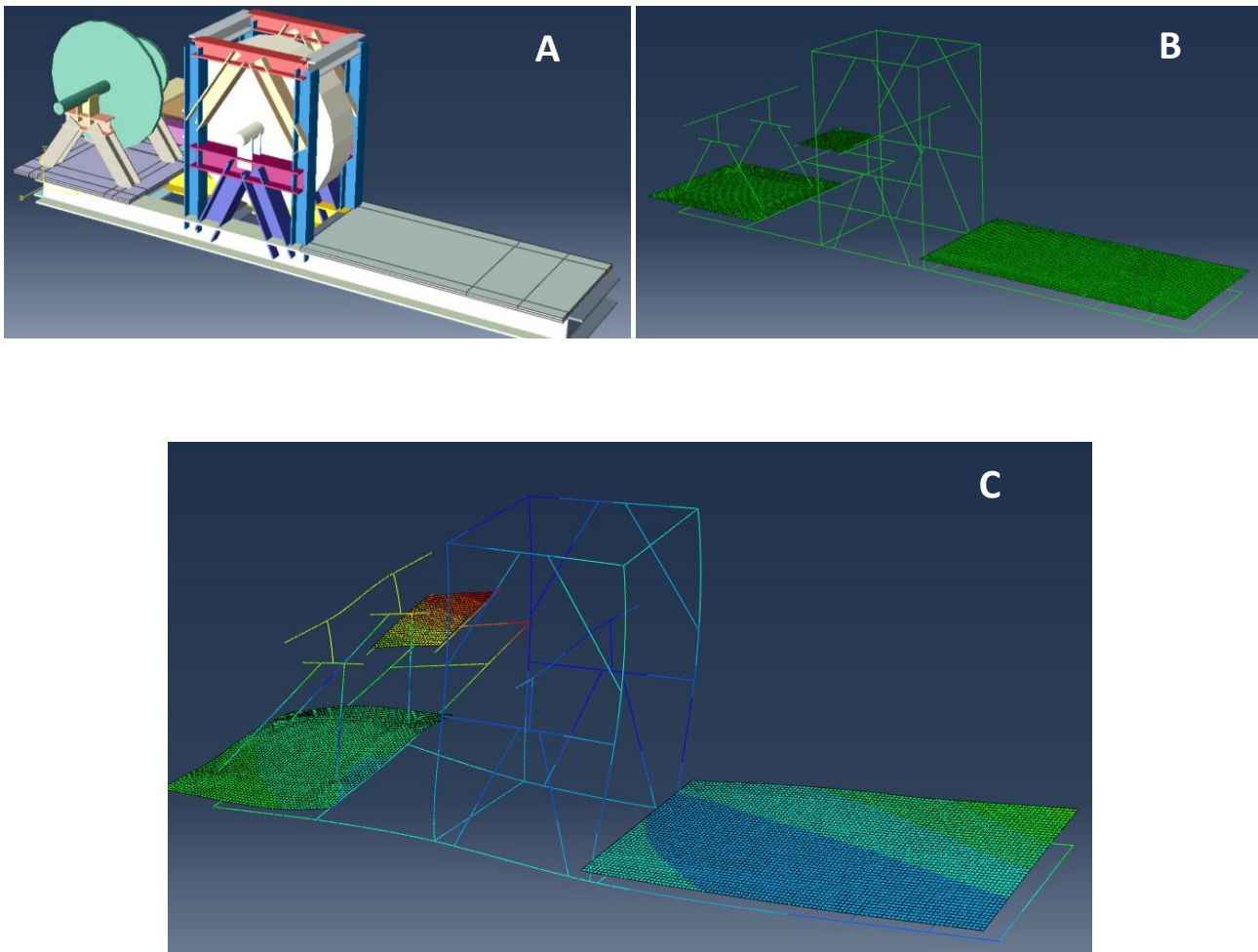
Fig. 8. A: Rendering of the FEM model of the dyno. B: FEM model of the dyno. C: Dyno deformation corresponding to the first relevant natural frequency.

3. Basic tests

The dynamometer has been characterized by running spin-down tests. This allows to record at a certain time the losses in the transmission and provide a reference for maintenance, in view of Industry 4.0 paradigms. In other words, by performing spin down tests (without a brake&wheel system involved) we monitor the status of the bearings, the status of the belt, and so on [37].

Two models have been developed to describe the spin down test. The first model is based on AMESIM and is shown in Fig. 9. In the AMESIM model all the single parts of BRAD are modelled, namely bearings, windage losses, belt efficiency.

The second model is analytical and is defined by the equation $F_x R_d + J_d \dot{\Omega} + M_l + M_{rr} = 0$ that can be rearranged as

$$J_d \ddot{\Theta} - a - c \dot{\Theta}^2 = 0 \qquad (5)$$

where $\Omega = \dfrac{d\Theta}{dt}$, a collects all of the terms of F_x, M_l, M_{rr} that do not depend on Θ (i.e. are constants), c collects all of the terms of F_x, M_l, M_{rr} that do depend on $\dot{\Theta}^2$

The *analytical* solution of equation (5) is

$$\Omega = \frac{\sqrt{a} \tanh\left(\sqrt{ac} * \left(t / J_d + \frac{\tanh^{-1}(\sqrt{c} v_0 / \sqrt{a})}{\sqrt{ac}} \right) \right)}{\sqrt{c}} \qquad (6)$$

Where

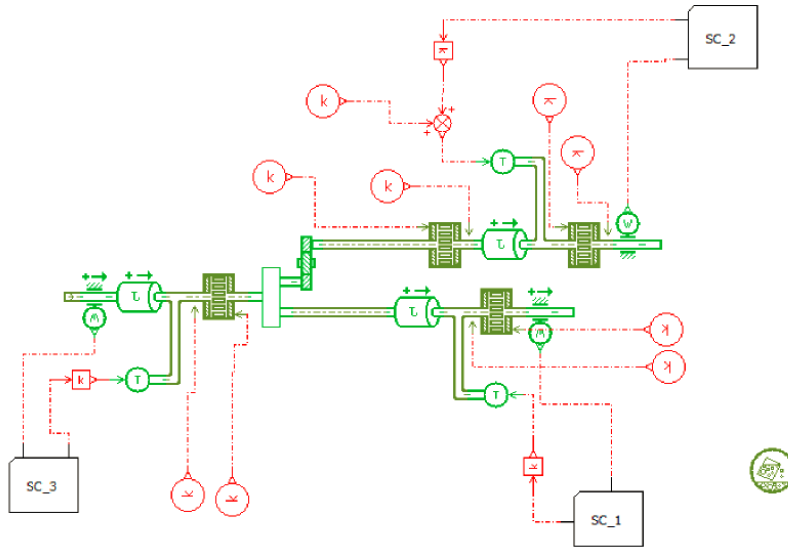J_d = 811

a = 53.3

c = 0.0204

Fig. 9. AMESIM model of BRAD.

In Fig. 10 the comparison of the two models is made. We see that, by a proper tuning of parameters *a* and *c*, the analytical model fits well the measurement. Monitoring *a* and *c* allows to monitor the status of BRAD and decide when maintenance has to be performed (i.e., substituting the belt, substituting the bearings, checking the alignment of axes and so on).
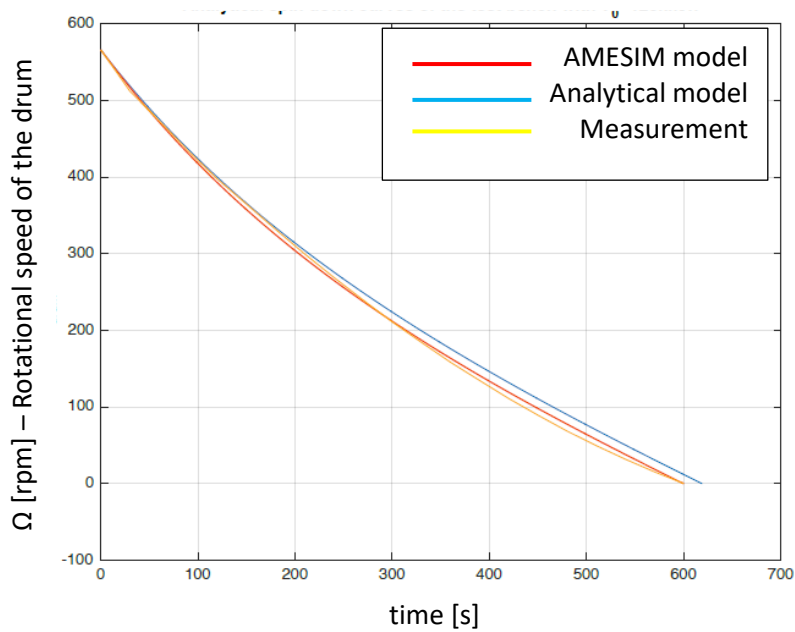

Fig.10. Spin down test of BRAD compared with the output of the AMESIM model and analytical model.

4. Typical tests

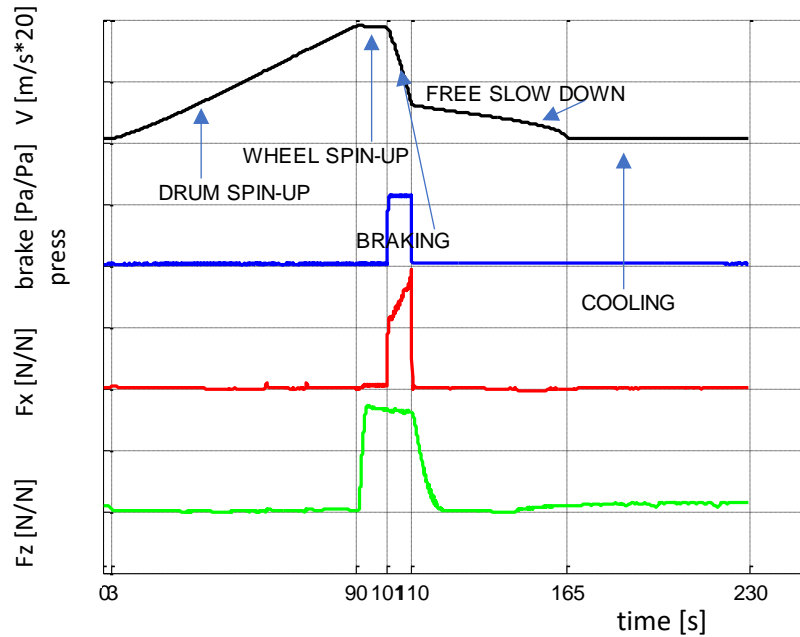### 4.1 Assessment of the deceleration

Fig.11. Typical brake test with BRAD.

Fig. 11 shows a typical test in which the brake&wheel system is activated and the drum is decelerated.

The typical test is started with a drum spin-up phase, in which the wheel is not in contact with the drum

and the initial speed is reached before the wheel is pushed against the drum for the wheel spin-up phase.

At this point, the driving motor is electrically disconnected and hydraulic pressure is delivered to the brake,

leading to the starting of the proper stop.

When final speed is reached (or drum is brought to a complete stop), pressure is dropped and the drum is

let spin down freely.

Vertical load on the wheel is also reduced for the cooling phase, in which the brake is let un-operated until

temperature is reasonably low for next application.

4.2 Assessment of the power dissipated by the brake

The bake-wheel system works as follows. Referring to Fig.1 A and to steady state, the input power into the wheel P_i and the output power from the wheel P_o read

$$P_i = F_x \Omega R_d$$
$$P_o = M_y \omega + M_{rr} \Omega$$

The difference between the input power and output power is due to the losses which are related to rolling resistance F_{rr}. The power dissipated by the rolling resistance is

$$F_{rr} \Omega R_d = P_i - P_o = F_x \Omega R_d - M_y \omega - M_{rr} \Omega$$

thus

$$F_{rr} = F_x - M_y \frac{\omega}{\Omega R_d} - \frac{M_{rr}}{R_d}$$

Considering the equilibrium of the wheel we can write (at steady state) $F_x = \dfrac{M_y + M_{rr}}{r}$. Introducing this expression into the above expression of F_{rr} and rearranging we find

$$F_{rr} = \frac{M_y}{r} \frac{\Omega R_d - \omega r}{\Omega R_d} + \frac{M_{rr}}{r} \frac{R_d - r}{R_d}$$

Since the longitudinal slip at the pneumatic tire of the wheel is [6] $s_x = \dfrac{\Omega R_d - \omega r}{\Omega R_d}$ we can write

$$F_{rr} = \frac{M_y}{r} s_x + \frac{M_{rr}}{r} \frac{R_d - r}{R_d}$$

If $s_x = 1$, i.e. the wheel is locked during braking and M_{rr} is vanishing, the rolling resistance becomes $F_{rr} = M_y/r$

which is just the longitudinal force $F_{rr} = F_x$.

If s_x is vanishing, and $R_d = \infty$, then $F_{rr} = M_{rr}/r$. If, from Fig.5, dz=0, then $F_{rr} = M_{rr}/r = F_z$ dx/r , from equilibrium

$F_{rr} = F_x$. The rolling resistance is again equal to the longitudinal force.

The actual working conditions occur at $0 < s_x < 1$, thus the rolling resistance F_{rr} is a part of F_x. In other words,

during braking, part of the power is dissipated by the wheel which helps the brake to perform its task.

In Fig. 12 a measurement of the power dissipated by the brake only and the measurement of the power

dissipated by the brake&wheel system are reported. The data are filtered with a lo pass filter (30Hz). A

moving average is also applied. In the considered time span of almost 20s, in which much of the braking

action occurs, the mean power dissipated by the brake is 132kW. The mean power dissipated by the brake

& wheel is 179kW. We see that nearly 30% of the brake power is dissipated by the wheel. According to the

knowledge of the Authors, this is an original result, both in the automotive and aerospace fields. Such a

measurement performed by the BRAD test rig appears to be unreferenced. Actually, in the classic literature

referring to vehicle dynamics [38-48] such a figure seems not properly highlighted. The result appears to be

meaningful because it has an impact on brake durability assessment and for repeated braking action, i.e.

thermal management of the brake&wheel system.
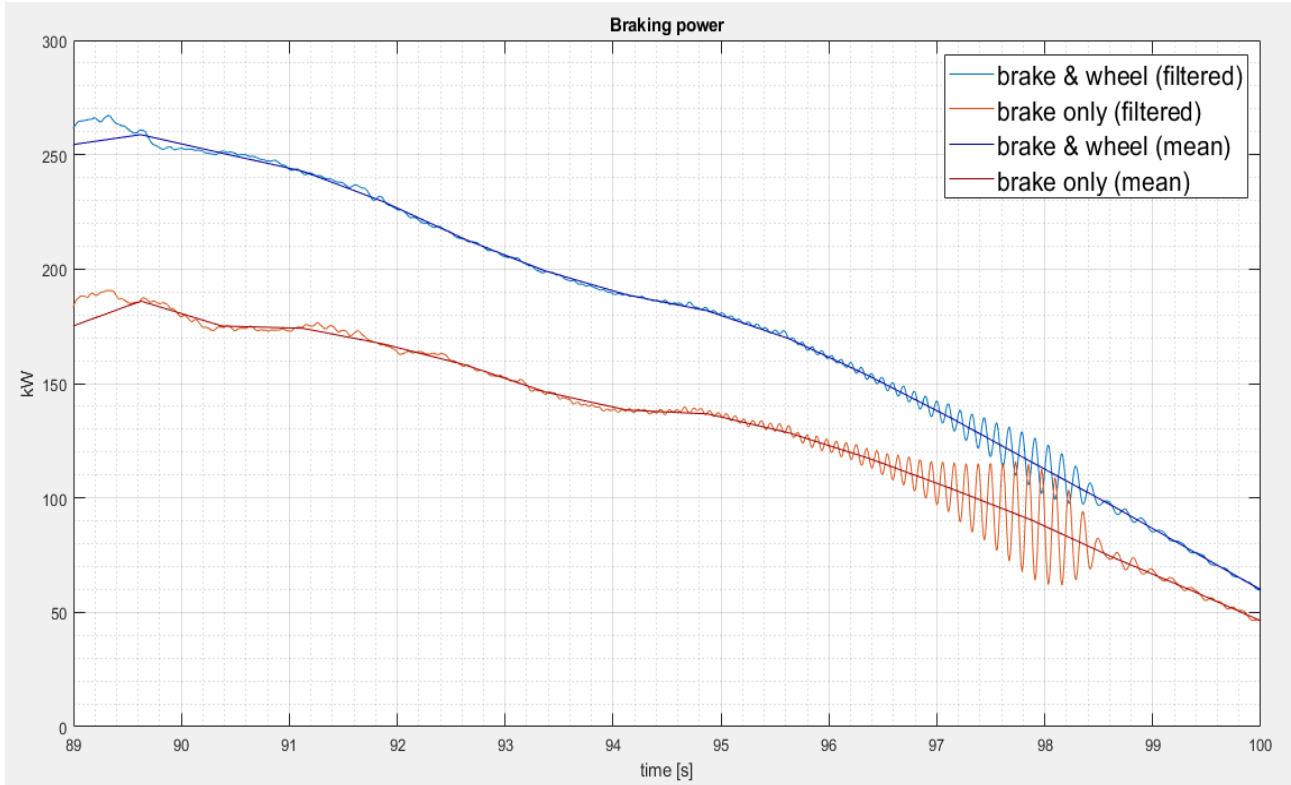
Fig. 12. Power dissipated by the brake and by the brake&wheel system.

5. Measurement accuracy

The evaluation of the accuracy of the measurement is quite straightforward. Actually, the quantities to be measured are

- the deceleration of the drum, $d_d = \dot{\Omega}\, R_d$

- the total power dissipated by the brake&wheel system $P_d = F_x\, \Omega\, R_d + M_{rr}\, \Omega$

- the power dissipated by the brake only $P_w = M_y\, \omega = (-J_w\dot{\omega} + Fr - M_{rr})\omega$

The uncertainty Δf of a generic measurement function $f(x_1, x_2, ..., x_n)$ can be calculated as $\Delta f =$

$\sqrt{\sum_{i=1}^{n} \left(\frac{\partial f}{\partial x_i} \Delta x_i \right)^2}$ (assuming that x_i are independent) where Δx_i is the uncertainty of x_i.

5.1 Linear deceleration of the drum

Referring to the deceleration of the drum d_d, the terms involved are $\dot{\Omega}$ and R_d. The uncertainty on $\dot{\Omega}$ is related on the measurement uncertainty on the drum encoder. The encoder adopted is a 4096 point/turn type so its uncertainty can be assumed as $2\pi/4096$. The drum speed is computed, by the acquisition system of the dyno, every 8.192e-3 s. The resulting uncertainty on $\dot{\Omega}$ is calculated in Tab. 5. The uncertainty on R_d is related to the measurement of a geometric quantity, performed by a measuring the drum external diameter by means of a FARO measuring arm. The uncertainty on R_d is 0.1 mm. The numerical value of the uncertainty on the deceleration of the drum d_d, is reported in Tab. 5. We see that the uncertainty is quite low, such a performance enables the dynamometer to measure accurately the kinematical behaviour of brake&wheel.

Table 5. Estimation of the measurement uncertainty of the drum linear deceleration d_d.

$f = d_d = \dot{\Omega}\,R_d$				
x_i	$\frac{\partial f}{\partial x_i}$	Δx_i	Reference value	$\left\| \frac{\partial f}{\partial x_i} \Delta x_i \right\|$
$\dot{\Omega}$	R_d	0.1 after proper data processing	8 rad/s²	0.6 * 0.1 = 0.06 m/s²
R_d	$\dot{\Omega}$	0.1e-3 m	0.6 m	8 * 0.1e-3 = 8e-4 m/s²
				$\Delta d_d = 0.06 \; m/s^2$

5.2 Power dissipated by the brake&wheel system

Referring to the power dissipated by the brake&wheel system, the terms involved are: F_x, Ω, R_d, M_{rr}.

The uncertainty on F_x value derives from equation (3) and is evaluated in Tab. 6.

Table 6. Estimation of the measurement uncertainty of the longitudinal force F_x.

$f = F_x = F_{LC1} + (F_{LC2} + F_{LC3}) - W$				
x_i	$\dfrac{\partial f}{\partial x_i}$	Δx_i	Reference value	$\left\lvert \dfrac{\partial f}{\partial x_i} \Delta x_i \right\rvert$
F_{LC1}	1	$10\ N$	-	$10\ N$
F_{LC2}	1	$5\ N$	-	$5\ N$
F_{LC3}	1	$5\ N$	-	$5\ N$
W	-1	$5\ N$	-	$5\ N$
				$\Delta F_x = 13{,}2\ N$

The measurement uncertainty of Ω can be evaluated according to Tab. 7.

Table 7. Estimation of the measurement uncertainty of the drum angular velocity Ω.

		$f = \Omega$		
x_i	$\dfrac{\partial f}{\partial x_i}$	Δx_i	Reference value	$\left\|\dfrac{\partial f}{\partial x_i}\Delta x_i\right\|$
Ω	1	$\left(\dfrac{2\,\pi}{4096}\right)/8.192e-3 = 0.187$ rad/s	-	0.187 rad/s
				$\Delta\Omega = 0.187\ rad/s$

The uncertainty on R_d has been already addressed above and it is $\Delta R_d = 0.1e-3\ m$.

The uncertainty on M_{rr} derives from equation 4 and has been evaluated in Tab. 8, the terms involved are W, X_{CG}, F_{LC2}, F_{LC3}, L_X .

Table 8. Estimation of the measurement uncertainty on the rolling resistance moment M_{rr}.

$$f = M_{rr} = - W * X_{CG} + (F_{LC2} + F_{LC3}) \, L_X - J_w d\omega/dt$$

x_i	$\dfrac{\partial f}{\partial x_i}$	Δx_i	Reference value	$\left| \dfrac{\partial f}{\partial x_i} \Delta x_i \right|$
W	$- X_{CG}$	$10\ N$	4000 N	$5\ Nm$
X_{CG}	$- W$	$1e-3\ m$	0.5 m	$4\ Nm$
F_{LC2}	$- L_x$	$5\ N$	1500 N	$5\ Nm$
F_{LC3}	$- L_x$	$5\ N$	1500 N	$5\ Nm$
L_x	$- F_{LC2} - F_{LC3}$	$1e-3\ m$	1 m	$3\ Nm$
				$\Delta M_{rr} = 10\ Nm$

Thus, the measurement uncertainty of P_d is calculated in Tab. 9.

Table 9. Estimation of the measurement uncertainty of the power dissipated by the brake&wheel system P_d.

$f = P_d = F_x\, \Omega\, R_d + M_{rr}\, \Omega$				
x_i	$\dfrac{\partial f}{\partial x_i}$	Δx_i	Reference value	$\left\|\dfrac{\partial f}{\partial x_i}\Delta x_i\right\|$
F_x	ΩR_d	$13\ N$	$10000\ N$	$0.5\ kW$
Ω	$F_x R_d + M_{rr}$	$0.187\ rad/s$	$70\ rad/s$	$2.1\ kW$
R_d	$F_x \Omega$	$1e-3\ m$	$0.6\ m$	$0.7\ kW$
M_{rr}	Ω	$10\ Nm$	$5000\ Nm$	$0.7\ kW$
				$\Delta P_d = 2.4\ kW$

Since the brake dissipates some MW, the uncertainty of 2.4 kW is quite low and reasonably we can state that the dynamometer is quite accurate.

5.3 Power dissipated by the brake only

Referring to the power dissipated by the brake only system, the terms involved are: J_w, $\dot{\omega}$, F_x, r, M_{rr}.

The uncertainty on J_w is related primarily to the measurement of the moment of inertia of the wheel. The uncertainty on this kind of measurement is typically 3 % of the measured value.

The uncertainty on $\dot{\omega}$ and ω can be assumed equal respectively to the uncertainty on $\dot{\Omega}$ and Ω, equal respectively to 0.1 rad/s² and 0.187 rad/s.

The uncertainty on F_x and M_{rr} have been already addressed above and are respectively 13 *N* and 10 *Nm*.

The uncertainty on *r* is related to the measurement of a geometric quantity, performed by means of a linear displacement sensor. The uncertainty on *r* can be assumed equal to 1e-3 *m*.

The uncertainty on P_w can be calculated as it is shown in Tab. 10.

Table 10. Estimation of the measurement uncertainty of the total power dissipated by the brake only P_w.

$$f = P_w = (-J_w\,\dot{\omega} + F_x\,r - M_{rr})\,\omega$$				
x_i	$\dfrac{\partial f}{\partial x_i}$	Δx_i	Reference value	$\left\lvert\dfrac{\partial f}{\partial x_i}\Delta x_i\right\rvert$
J_w	$\dot{\omega}\,\omega$	$0.015\ kg\ m^2$	0.5 kg m²	$0.04\ kW$
$\dot{\omega}$	$J_w\,\omega$	$0.1\ rad/s^2$	$18\ rad/s^2$	$1.7\ kW$
F_x	$r\,\omega$	$13\ N$	10000 *N*	$0.5\ kW$
r	$F_x\,\omega$	$1e-3\ m$	$0.28\ m$	$1.5\ kW$
M_{rr}	$-\omega$	$10\ Nm$	5000 *Nm*	$1.5\ kW$
ω	$J_w\,\dot{\omega} + F_x\,r - M_{rr}$	$0.187\ rad/s$	$150\ rad/s$	$0.4\ kW$
				$\Delta P_w = 2.8\ kW$

Since the brake dissipates some MW, the uncertainty of 2.8 kW is quite low and reasonably we can state that the dynamometer is quite accurate.

6. Conclusion

A new dynamometer for brake&wheel performance assessment has been presented. A pneumatic wheel is pressed on a drum and rotates with it. The drum is connected to a system (transmission and flywheels) that reproduces the inertia of the vehicle whom the brake under test belongs to. As the brake is activated, the wheel applies a longitudinal force to the drum that is decelerated until the rest condition is reached.

The dynamometer has an unreferenced architecture, which allows to measure the power dissipated by the assembly wheel plus brake or to measure the power dissipated by the brake only. Such a feature makes the dynamometer a quite unique test rig.

The measured variables coming from kinematic sensors, load cells and geometric data are processed to obtain the linear deceleration of the drum, the longitudinal force at wheel-drum interface, the drum angular velocity, the rolling resistance moment at the wheel, the power dissipated at the brake and wheel assembly, the power dissipated at the brake only. All of the measurement uncertainties are derived and discussed.

We have shown that the wheel can dissipate up to 30% of the power dissipated by the brake only. This conclusion is unreferenced and quite significant both in the automotive and aerospace fields. The new dynamometer allows to obtain very accurate and precise information for brake design.

Literature

[1] Link, www.linkeng.com

[2] MTS, www.mts.com

[3] Horiba, www.horiba.com

[4] E Galindo et Al., Chassis Dynamometer Testing: Addressing the Challenges of New Global Legislation, SAE International, 2107, R-452, ISBN 978-0-7680-8278-4

[5] Association of American Railroads, Railroad wheel dynamometer (91st national historic mechanical engineering landmark). url: https://www.asme.org

[6] ETSO C26 C: AIRCRAFT WHEELS AND WHEEL-BRAKE ASSEMBLIES (CS-23, -27 and -29 aircraft)

[7] TSO C26D: Aircraft Wheels, Brakes and Wheel/Brake Assemblies for parts 23, 27 and 29 aircraft

[8] SAE ARP5381: Minimum Performance Recommendations for Part 23, 27, and 29 Aircraft Wheels, Brakes, and Wheel and Brake Assemblies

[9] ETSO C135a: LARGE AEROPLANE WHEELS AND WHEEL AND BRAKE ASSEMBLIES

[10] N. Yu. Kuznetsov, A. I. Fedotov, and V. G. Vlasov, Test benches for studying the properties of car tyres, AIP Conference Proceedings 1915, 040031 (2017); doi: 10.1063/1.5017379

[11] K. Zhou et al., "Research on Vehicle ABS Detection Technology Based on Flywheel Inertia Simulation", Advanced Materials Research, Vols. 765-767, pp. 2117-2122, 2013

[12] Wang, R., Liu, Z., Ma, Y., Qi, Z., Improvement design of brake dynamometer, Nongye Jixie Xuebao/Transactions of the Chinese Society of Agricultural Machinery, 37 (6), pp. 17-19, 2006

[13] . Kruger, L.K., Boss, K., Angerer, S.J., Brake test rig for operating load simulation, XVIII FISITA Congress - The Promise of New Technology in the Automotive Industry; Torino, Italy; ; May 1990; Code 13957, Proceedings - Society of Automotive Engineers, 1990, Pages 383-388

[14] https://www.fast.kit.edu/download/DownloadsFahrzeugtechnik/Testing_facilities_KIT-FAST-LFF.pdf

[15] https://www.ika.rwth-aachen.de/en/research/equipment/testing-facilities/drive-systems/332-four-wheel-test-bench.html

[16] J-H Abendroth, U Schwarz, Correlating Dynamometer and Vehicle Brake Test Results: Brake Squeal, SAE Technical Paper2001-01-3143DOI: https://doi.org/10.4271/2001-01-3143

[17] Braking System Dynamics, A-5A Wheels, Brakes and Skid Controls Committee, Aerospace Standard AIR1064D, SAE, 2016

[18] J P Medzorian, M A Shea, Dynamometer Simulation of Aircraft Tire Wear Due to Braking, SAE Technical Paper2001-01-3028DOI: https://doi.org/10.4271/2001-01-3028, 2001

[19] Gobbi, M., Mastinu, G., Ballo, F., and Previati, G., "Race Motorcycle Smart Wheel," SAE Int. J. Passeng. Cars - Mech. Syst. 8(1):119-127, 2015, https://doi.org/10.4271/2015-01-1520.

[20] Mastinu, G., Gobbi, M., Previati, G., A New Six-axis Load Cell. Part I: Design ,Experimental Mechanics 51(3), pp. 373-388, 2011

[21] Gobbi, M., Mastinu, G., Giorgetta, F. Sensors for measuring forces and moments with application to ground vehicle design and engineering, American Society of Mechanical Engineers, Design Engineering Division (Publication) DE, 118 A (1), pp. 161-168, 2005.

[22] Gobbi, M., Mastinu, G., Previati, G., and Pennati, M., "6-Axis Measuring Wheels for Trucks or Heavy Vehicles," SAE Int. J. Commer. Veh. 7(1):141-149, 2014, https://doi.org/10.4271/2014-01-0816.

[23] Grochowicz, J., Agudelo, C., Reich, A., Wollenweber, K. et al., Brake Dynamometer Test Variability Analysis of Root Causes, SAE paper 2010-01-1697, 2010

[24] Grochowicz, J., Agudelo, C., Reich, A., Wollenweber, K. et al., Brake Dynamometer Test Variability Part 2- Description of the Influencing Factors, SAE Int. J. Passeng. Cars – Mech. Syst. 4(3):1394-1421, 2011,

[25] Mallya, B.V., Brake block dynamometer laboratory of the indian railways, Journal of the Institution of Engineers (India): Mechanical Engineering Division, 57 pp. 186-192, 2017

[26] Augsburg, K., Savitski, D., Heidrich, L., and Ivanov, V., "Combined Testing Technique: Development of Friction Brake System for Electric Vehicle," SAE Technical Paper 2014-01-2529,

https://doi.org/10.4271/2014-01-2529, 2014

[27] Grochowicz, J., Agudelo, C., Li, S., Abendroth, H. et al., "Influence of Test Procedure on Friction Behavior and its Repeatability in Dynamometer Brake Performance Testing," SAE Int. J. Passeng. Cars - Mech. Syst. 7(4):2014, doi:10.4271/2014-01-2521.

[28] Zimmer, D., "ATE Friction Test Machine and Other Methods of Lining Screening," SAE Technical Paper 820163, 1982, doi:10.4271/820163.

[29] Krough, B., Dyar, L., and Bray, P., "Adapting On-vehicle Brake Drag Testing to a Bench Dynamometer," SAE Technical Paper 2011-01-2376, 2011, https://doi.org/10.4271/2011-01-2376.

[30] Loh, W., Basch, R., Dalka, T., and Hartsock, D., "Development of a Brake Dynamometer-Vehicle Model Hardware-in-the-Loop System," SAE Technical Paper 2003-01-3337, 2003, https://doi.org/10.4271/2003-01-3337.

[31] Wang, R., Wang, B., Sun, H., Development of a single wheel test bench for anti-lock brake system, Proceedings, International Conference on Optoelectronics and Image Processing, ICOIP 2010 1,5663001, pp. 429-431

[32] Ma, J., Wu, B., Liu, X., and Sun, J., "A New Method of Inertia Simulation in Brake Dynamometer Testing," SAE Technical Paper 2008-01-2578, 2008, https://doi.org/10.4271/2008-01-2578.

[33] Thompson, J., Marks, A., and Rhode, D., "Inertia Simulation in Brake Dynamometer Testing," SAE Technical Paper 2002-01-2601, 2002, https://doi.org/10.4271/2002-01-2601.

[34] Haataja, M. and Leinonen, T., "The Quality Requirements of a Roller Brake Dynamometer Measurements," SAE Technical Paper 2002-01-3140, 2002, https://doi.org/10.4271/2002-01-3140.

[35] Hendrichs, W., Dimensioning and Comparing Inertia Type Brake Dynamometers. (in German), Zeitschrift fuer Eisenbahnwesen und Verkehrstechnik - Glasers Annalen 112(5), 1988

[36] Steis, D., "Inertia Brake Dynamometer Testing Techniques for FMVSS 121," SAE Technical Paper 751010, 1975, https://doi.org/10.4271/751010.

[37] R Filisetti, Progettazione, simulazione e messa in opera di un banco prove per freni, Thesis Dissertation, Politecnico di Milano, 2016.

[38] Mastinu, G., Ploechl M, Road and Off-road vehicle system Dynamics Handbook, CRC Press, Boca Raton, New York, USA, 2014

[39] Gillespie, T.D., et Al., Roll dynamics of commercial vehicles, Vehicle system Dynamics vol.9, 1980, pp 1-17[40] Genta, G., Motor vehicle dynamics, modelling and simulation, Levrotto&Bella Turin, 1997

[41] Mitschke, M, Wallwntowitz, H., Dynamik der Kraftfahrzeuge, Springer, Berlin 2004

[42] Pacejka, H., Tyre and vehicle dynamics, SAE International and Elsevier, 2005

[43] Clarks, S. (Ed.) Mechanics of Pneumatic Tyres, U.S. Department of Transportation. National Highway Traffic Safety Administration (1980)

[44] Dixon J.C. Tires, suspension and handling, Society of Automotive Engineers, Warrendale-United State, 1996.

[45] Howard G., Whitehead J.P., Bastow D. Car Suspension and Handling (Fourth Edition), 2004, SAE, Warrendale-PA-USA.

[46] Gent, A., Walter, D. The Pneumatic Tire, DOT NHTSA, 2006

[47] Guiggiani, M., The Science of Vehicle Dynamics, Springer Vlg., Berlin, 2014

[48] W F Milliken, D L Milliken, Race car vehicle dynamics, SAE International, Warrendale, USA, 1994

Appendix

Table A1. Technical specifications of the main sensors used in the BRAD test rig

LOAD CELLS

	S2tech 546 QDT	S2tech 546 QDT	Pavone Sistemi 60001
Full Scale	10000 N	20000 N	50000 N
Rated output	2mV/V	2mV/V	3mV/V
Non-repeatability	< ±0,033 % FS	< ±0,033 % FS	< ±0,010 % FS
Total accuracy	< ±0,046 % FS	< ±0,046 % FS	< ±0,020 % FS
Power supply	10 Vcc/ac	10 Vcc/ac	10 Vcc/ac
Bridge resistance	350 Ω	350 Ω	350 Ω
Safe overload	125 % FS	150 % FS	150 % FS
Failure overload	300 % FS	300 % FS	300 % FS
Operating temperature	-20/+70 °C	-20/+70 °C	-18/+65 °C
Compensated temperature	-10/+40 °C	-10/+40 °C	-10/+40 °C
Temperature shift zero	< ±0,046 % FS	< ±0,046 % FS	< ±0,001 % FS /°F
Material	Steel	Steel	Steel
Mass	1.1 kg	2.0 kg	3.1 kg

ENCODER

Technical data - electrical ratings	
Voltage supply	4.75...30 VDC (Vout = 5 VDC)
Reverse polarity protection	Yes
Short-circuit proof	Yes
Consumption w/o load	≤70 mA
Initializing time	≤30 ms after power on
Pulses per revolution	1...65536
Scan ratio	45...55 % typical at 1024, 2048 ppr
Reference signal	Zero pulse 90° or 180°
Sensing method	Optical
Output frequency	≤300 kHz (TTL) ≤160 kHz (HTL)
Output signals	A+, B+, R+, A-, B-, R-
Output stages	TTL/RS422 HTL/push-pull
Programmable parameters	Output level TTL/HTL Pulse number 1...65536 Zero pulse width 90°/180° Zero pulse position Signal sequence
Interference immunity	DIN EN 61000-6-2
Emitted interference	DIN EN 61000-6-3
Approval	UL 508 / CSA 22.2
Technical data - mechanical design	
Size (flange)	ø58 mm
Shaft type	ø12 mm, clamping ring at A side
Motor shaft tolerance	0.2 mm axial 0.03 mm radial
Protection DIN EN 60529	IP 65 (without shaft seal)
Operating speed	≤6000 rpm (+20 °C, IP 65)
Starting torque	≤0.02 Nm (+20 °C, IP 65)
Material	Housing: aluminium die-cast Flange: aluminium
Operating temperature	-40...+100 °C
Relative humidity	90 % non-condensing
Resistance	DIN EN 60068-2-6 Vibration 30 g, 10-2000 Hz DIN EN 60068-2-27 Shock 250 g, 6 ms
Connection	Flange connector M12, 8-pin
Weight approx.	300 g